Transient climate sensitivity shaped by low cloud changes remotely driven by Southern Ocean processes

Robert R. Ford,[a] , Brian E. J. Rose,[a] and M. Cameron Rencurrel,[a]

[a] *Department of Atmospheric and Environmental Sciences, University at Albany, State University of New York, Albany, New York*

Corresponding author: Robert R. Ford, rford2@albany.edu

Early Online Release: This preliminary version has been accepted for publication in *Journal of Climate*, may be fully cited, and has been assigned DOI 10.1175/JCLI-D-24-0164.1. The final typeset copyedited article will replace the EOR at the above DOI when it is published.

ABSTRACT: Transient climate sensitivity is strongly shaped by geographical patterns of ocean heat uptake (OHU). To isolate the effects of uncertainties associated with OHU, a single slab ocean model is forced with doubled CO_2 and an ensemble of OHU patterns diagnosed from transient warming scenarios in 12 fully-coupled models. The single-model ensemble produces a wide range of Southern Ocean (SO) sea surface temperature (SST) and Antarctic sea ice responses, which are in turn associated with a 1.1–2.0 K range of transient climate response (TCR). Feedback analysis attributes the TCR spread primarily to shortwave effects of low clouds in the Southern Hemisphere (SH) midlatitudes. These cloud changes are strongly positively correlated with storm track eddy kinetic energy. It is argued that midlatitude clouds (and thus planetary albedo) are remotely driven by SO SST and Antarctic sea ice, mediated by large-scale changes in SH baroclinicity and lower-tropospheric stability. The robustness of this atmospheric teleconnection between SO SST, Antarctic sea ice, and global feedback through midlatitude clouds is supported through additional simulations that explore more extreme SST and sea ice perturbations. These results highlight the importance of understanding physical relationships between SST, sea ice, circulation, and cloud changes in the SH as a pathway to better constraining transient climate sensitivity.

Accepted for publication in *Journal of Climate*. DOI 10.1175/JCLI-D-24-0164.1.

SIGNIFICANCE STATEMENT: Although it is well known that Earth's global-mean surface temperature increases with increasing atmospheric CO_2, there are still significant uncertainties in the temperature and sea ice trends over the Southern Ocean region. Using a climate model, we find that Southern Ocean temperature and Antarctic sea ice changes can result in substantial cloud cover changes over the Southern Hemisphere, which play a primary role in determining the amount of warming in our experiments. We suggest that, in order to reduce uncertainty in future climate change, more work is needed to understand how the climate of the southern polar region can affect the circulation and clouds of the midlatitudes.

1. Introduction

Reducing uncertainty in climate sensitivity, defined as the global-mean surface temperature (GMST) response to a radiative forcing, has become a central goal of climate science. The two most common metrics of climate sensitivity are equilibrium climate sensitivity (ECS), defined as the equilibrium (i.e., as net TOA radiation approaches zero) GMST response to an instantaneous doubling of CO_2, and transient climate response (TCR), defined as the GMST response to a 1% per year CO_2 ramp at the time of doubling. The latest IPCC report gives a likely range of 2.5–4.0 K for ECS and 1.4–2.2 K for TCR (Forster et al. 2021). While ECS provides a useful benchmark for comparing sensitivity estimates from models, historical observations, and paleoclimate records, TCR allows us to take into consideration the effect of variations in ocean heat uptake (OHU), which are known to influence the strength of feedbacks (Rugenstein et al. 2016; Rose and Rayborn 2016).

a. Pattern effects and low cloud feedbacks

The largest sources of uncertainty in climate sensitivity are the various cloud feedbacks (Sherwood et al. 2020). Uncertainties in the responses of different types of clouds do not only come from differences in cloud physics across models; they also stem from uncertainties in the patterns of surface warming that are coupled to the clouds. This is one of the main contributors to the pattern effect, which refers to the coupling of radiative feedbacks and spatial surface temperature patterns (Dong et al. 2020). Notably, uncertainty in the temperature trends of the Southern Ocean (SO) and eastern Pacific (EP) under increasing CO_2 forcing contributes substantially to the uncertainty in global cloud feedbacks (Kang et al. 2023). While models tend to show enhanced warming over the

Accepted for publication in *Journal of Climate*. DOI 10.1175/JCLI-D-24-0164.1.

SO and EP, observations show little warming over the same regions (Wills et al. 2022). A recent focus in the literature has been on changes in the zonal sea surface temperature (SST) gradient in the equatorial Pacific and the resulting cloud and lapse rate feedbacks (Lee et al. 2022).

Previous studies (Hwang et al. 2017; Kim et al. 2022; Dong et al. 2022) have explored a teleconnection between the SO and tropical EP through which cold anomalies can be advected equatorward, contributing to enhanced cloudiness in the EP attributable to increased lower-tropospheric stability (Wood and Bretherton 2006). This may explain why the EP is colder than models suggest it should be, but there are still uncertainties in the sources of the SO cooling, including the roles of Antarctic meltwater (Rye et al. 2020), ozone depletion (Hartmann 2022), and internal variability (Chung et al. 2022). As will be described in more detail in the following sections, we produced an ensemble of runs of the slab ocean configuration of the Community Earth System Model (CESM) whose range of TCR can be primarily attributed to a range of SO SST and Antarctic sea ice responses, induced by various patterns of OHU. Thus, we have an ensemble that represents a realistic spread in the SO environment, and this allows us to explore the physical mechanisms through which the SO impacts the entire Southern Hemisphere (SH), particularly the midlatitudes.

There is agreement across models of a poleward shift in the midlatitude jet and storm tracks under CO_2 forcing (Ceppi et al. 2014; Voigt et al. 2021), and models, including CESM, generally exhibit a dipole pattern around 45°S in the shortwave (SW) cloud feedback in the midlatitudes following warming, with increased reflection poleward and decreased reflection equatorward (Kay et al. 2014). However, by calculating the component of the SW cloud radiative effect that could be attributed to a jet shift in CMIP5 under transient forcings, Ceppi and Hartmann (2015) showed that these SW cloud changes are not the result of the poleward shift in the midlatitude jet. The negative SW cloud feedback on the poleward side has been attributed to a brightening of the clouds through increased liquid water path (Ceppi et al. 2016), while the positive SW cloud feedback on the equatorward side is the result of a decrease in low cloud amount (Sherwood et al. 2020), usually attributed to the thermodynamic and stability mechanisms outlined by Bretherton (2015). Given that these processes are not well understood, we will examine the relationships between midlatitude circulation changes and SW cloud feedbacks in our simulations.

Accepted for publication in *Journal of Climate*. DOI 10.1175/JCLI-D-24-0164.1.

b. Research objectives

This research originally began with the question: how much of the spread in TCR across fully-coupled models can be explained by inter-model differences in OHU patterns? This motivated our experimental design of using a single slab ocean model forced with a diversity of OHU patterns diagnosed from CMIP5. Our original goal was to directly attribute the spread in temperature response across our ensemble to patterns of OHU through a framework such as OHU efficacy (Winton et al. 2010; Rose et al. 2014). The complexity of the Antarctic sea ice response to the imposed OHU limited our ability to make such an attribution. Instead, the simulations present an opportunity to investigate transient warming scenarios with a range of SO responses. So we address a question of crucial importance for understanding cloud feedbacks in the face of uncertain temperature trends and forcing mechanisms in the SO: given a plausible range of SO SST and Antarctic sea ice responses, what mechanisms are responsible for the resulting spread in TCR?

The rest of this paper is organized as follows. In section 2, we describe the model used and the experimental setup. In section 3, we summarize the temperature, sea ice, and circulation response to the prescribed forcing. In section 4, we describe the feedbacks responsible for the spread in model response. Section 5 explores the mechanisms behind the range of feedbacks, and in section 6, we discuss the implications of the results and conclude.

2. Model configuration and experiments

We use the slab ocean version of the Community Earth System Model, version 1.2.1 (CESM1), consisting of the Community Atmosphere Model, version 5 (CAM5), the Community Land Model, version 4 with carbon–nitrogen biogeochemistry (CLM4-CN), the Community Ice Code (CICE), and the data slab ocean model (DOCN-SOM). We run an 80-year control simulation with prescribed pre-industrial values of CO_2 (284.7 ppm) and a monthly ocean heat flux divergence (Q-flux) forcing generated from a 20-year average of the fully-coupled version of the CESM1-CAM5 pre-industrial control simulation. The annual-mean Q-flux for this control simulation is shown in Fig. 1a. It is primarily characterized by heat flux into the ocean in the equatorial regions and heat fluxes into the atmosphere in the North Atlantic, associated with surface deep water formation, and along continental boundaries, associated with the poleward transport of warm, subtropical water. The

Accepted for publication in *Journal of Climate*. DOI 10.1175/JCLI-D-24-0164.1.

Southern Ocean is also a weak heat source. Because the control simulation has reached equilibrium, there is zero net heat flux into the ocean from the atmosphere.

a. Diagnosed CMIP5 OHU

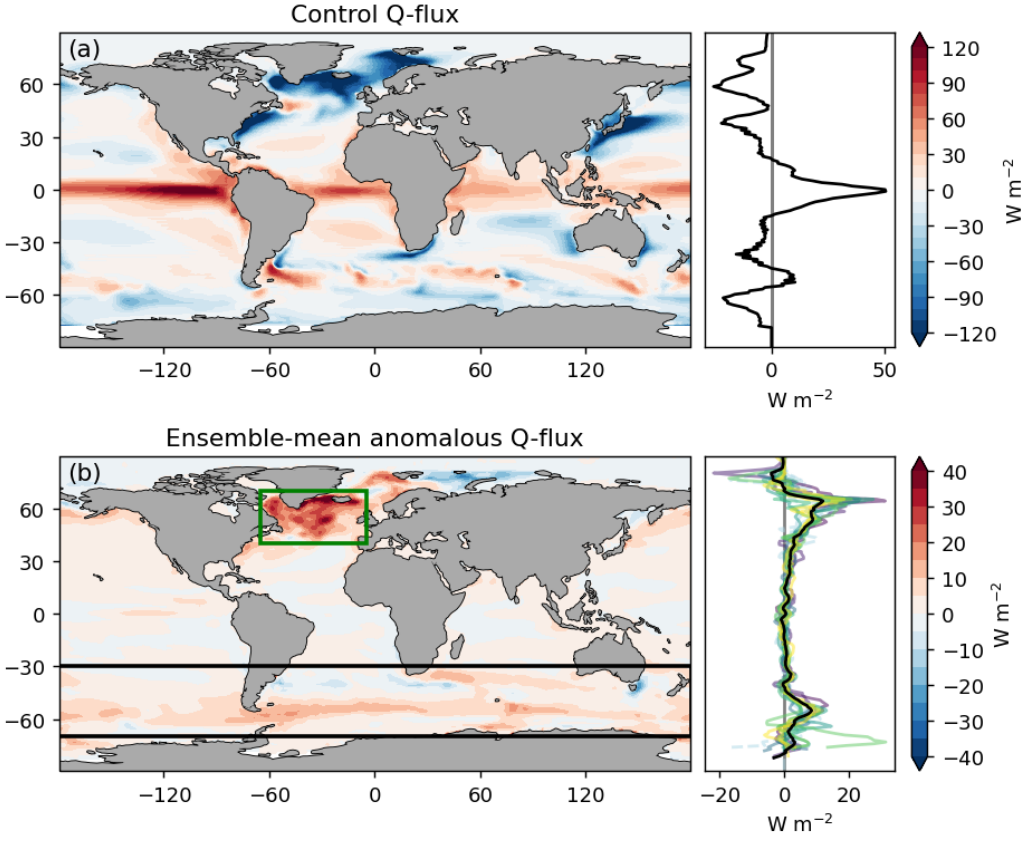

FIG. 1. (a) Control and (b) ensemble-mean anomalous Q-flux forcing patterns (annual mean). In the zonal-mean plots, the black lines correspond to the Q-flux maps shown, while the other lines correspond to the individual Q-flux patterns. Maps of each Q-flux pattern are shown in Fig. A1.

Rugenstein et al. (2016) showed that steady states from a slab ocean model can be used to approximate transient results from a fully-coupled model when the surface heat flux generated from the fully-coupled model is prescribed at the bottom of the slab ocean as a heat flux divergence, which represents heat transfer between the mixed-layer and deep ocean (i.e., OHU). The goal of this method is to recreate the transient climate state from a fully-coupled climate model in a slab ocean model. The transient climate state can be thought of as being the response to two forcings at

Accepted for publication in *Journal of Climate*. DOI 10.1175/JCLI-D-24-0164.1.

the time of CO_2 doubling: the positive downward forcing from doubled CO_2 and the OHU forcing that removes energy from the surface to the deep ocean. By allowing the slab ocean model to come into equilibrium with the combined forcing, we ensure that the net surface heat flux exactly balances the imposed OHU, and thus matches the surface heat flux of the fully-coupled model from which the OHU pattern was diagnosed. By the same logic, it is appropriate to abruptly double the CO_2 rather than apply a gradual forcing ramp since we are seeking the equilibrium response of the slab ocean model to the combined forcing. As will be described in more detail in the next section, the resulting warming pattern is substantially different from the equilibrium warming to $2xCO_2$ alone and much more closely resembles the transient warming patterns of fully coupled models, including reduced global mean warming and only a slight warming of the SH extratropics.

We follow this methodology by generating Q-flux forcing patterns from 15 fully-coupled CMIP5 models listed in Table 1. To do this, we calculate the anomalous monthly-mean values in the downward surface heat flux in seawater (hfds in CMIP nomenclature, consisting of both the surface heat flux and the heat flux from sea ice formation/melting) associated with the TCR of each model. That is, we take the difference between the 20-year monthly-mean hfds at the time of a transient doubling of CO_2 in the 1pctCO2 simulations (years 60-80) and the climatological monthly-mean hfds of the piControl simulations, calculated using the maximum available (up to 1600-year) output. It is typical to use the 20-year average around year 70 in 1pctCO2 simulations in order to minimize the influence of internal variability while still capturing the response at year 70 (Dufresne and Bony 2008; Meehl et al. 2020). The annual- and ensemble-mean is shown in Fig. 1b. These are then added directly to the CESM1-CAM5 control Q-flux pattern to be applied to the model.

The CMIP5 models used in this study were chosen based on data availability at the time when our CESM1-CAM5 experiments were run. One could also generate and prescribe Q-flux patterns from the CMIP6 ensemble. However, we would not expect the results to be meaningfully different, since this study focuses on the mechanisms responsible for the range of responses in CESM1-CAM5 to the Q-flux patterns, not the Q-flux patterns themselves. It is important to note that intrinsic to this slab ocean analysis is a temporally-averaged constant mixed-layer depth, which is prescribed in the Q-flux forcing files. Sallée et al. (2013) found that CMIP5 simulations have a wide range of mixed-layer depths, particularly in the Southern Ocean, potentially influencing the seasonality and the annual mean of the anomalous OHU values. In these simulations, we choose to keep the

Accepted for publication in *Journal of Climate*. DOI 10.1175/JCLI-D-24-0164.1.

TABLE 1. Models used, TCR of each (Flato et al. 2013), and CESM1-SOM TCR with the models' Q-fluxes applied. Note that the TCR of CNRM-CM5-2 is missing from Flato et al. (2013). Asterisks denote +ΔSIC runs.

Model	CMIP5 TCR (K)	CESM1-SOM TCR (K)
BNU-ESM	2.6	1.1
MIROC-ESM	2.2	1.2
NorESM1-ME	1.6	1.4
INM-CM4	1.3	1.5
MRI-CGCM3	1.6	1.6
CESM1(BGC)	1.7	1.6
NorESM1-M	1.4	1.7
BCC-CSM1.1(m)	2.1	1.7
CNRM-CM5-2	–	1.8
CCSM4	1.8	1.9
BCC-CSM1.1	1.7	2.0
CSIRO-Mk3.6.0	1.8	2.0
Mean	1.8	1.6
CNRM-CM5*	2.1	-0.8
MIROC5*	1.5	0.5
ACCESS1.3*	1.7	0.9

prescribed mixed-layer depth constant across all runs, calculated from the CESM1-CAM5 control simulation alongside the control Q-flux.

b. Slab ocean CESM1-CAM5 runs

We run each Q-flux experiment of the slab ocean CESM1-CAM5 (hereafter CESM1-SOM) with an abrupt doubling of CO_2 for 40 years. Since the slab ocean model equilibrates quickly (around 20 years; Danabasoglu and Gent 2009), we take the average of the last 20 years minus the pre-industrial control state as the response, approximating TCR. Somewhat surprisingly, three out of 15 prescribed Q-flux patterns (generated from CNRM-CM5, MIROC5, and ACCESS1.3) resulted in global average sea ice growth (Fig. A3, top row), which we use as a heuristic cutoff for a "realistic" response. We denote those three Q-flux patterns and their corresponding responses in CESM1-SOM as "+ΔSIC" and separate them from averages and correlations, since their inclusion would significantly inflate correlations that might otherwise be weak across the warmer, more realistic runs. Instead, they will primarily be analyzed alongside the 12-member ensemble for a qualitative comparison.

Accepted for publication in *Journal of Climate*. DOI 10.1175/JCLI-D-24-0164.1.

TABLE 2. Summary of experiments.

Experiment name	CO_2	Q-flux	Number of runs	Approximates
Control	1x	Climatology	1	–
2xCO2 only	2x	Climatology	1	ECS
Ensemble	2x	CMIP5 anom. + clim.	12	TCR
+ΔSIC	2x	CMIP5 anom. + clim.	3	–
CM Q-flux	2x	Ensemble-mean anom. + clim.	1	TCR

We run an additional experiment with the average Q-flux of the 12-member ensemble (denoted "CM Q-flux") to test the linearity of the Q-flux forcing method, as well as a run with doubled CO_2 and the control Q-flux (denoted "2xCO2 only") to approximate ECS for comparison. These experiments are summarized in Table 2.

3. Temperature, sea ice, and circulation responses

The spread in TCR from our 12-member ensemble (1.1–2.0 K, mean 1.6 K) is very similar to the TCR spread of the same 12 fully-coupled CMIP5 models (1.3–2.6 K, mean 1.8 K; Flato et al. 2013). However, the corresponding CESM1-SOM and CMIP5 responses are not well correlated ($r = -0.42$; compare the second and third columns of Table 1). If these two ensembles were perfectly correlated, then it would imply that TCR is completely determined by the particular OHU pattern. The lack of correlation here implies that (1) the details of the OHU patterns do not have a significant impact on TCR compared to other differences across models and/or (2) unrealistic interactions between OHU, mixed-layer depth, and sea ice are masking the impact of OHU patterns. So, it is probably not correct to interpret these results as CESM1-SOM isolating the effect of OHU on TCR across the CMIP5 ensemble.

By the OHU efficacy framework (Winton et al. 2010; Rose et al. 2014), we might expect that high-latitude OHU would be a good predictor of the temperature response, but the mean Q-fluxes over the areas of large OHU (the Southern Ocean and North Atlantic), as well as the global-mean Q-flux, are not well-correlated with the temperature response (Fig. 2). Note that most of the weak negative correlation between TCR and OHU in the SO and globally is primarily the result of the two coldest ensemble members (forced by BNU-ESM and MIROC-ESM Q-fluxes) having the

Accepted for publication in *Journal of Climate*. DOI 10.1175/JCLI-D-24-0164.1.

greatest heat uptake. The inclusion of the three +ΔSIC runs in Fig. 2 highlights the fact that their cold response is not simply the result of unusually high OHU over a large area.

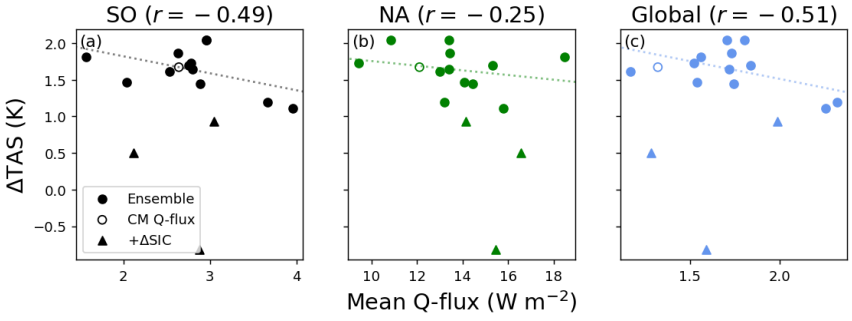

FIG. 2. Correlations between Southern Ocean (Fig. 1b black box), North Atlantic (Fig. 1b green box), and global-mean Q-flux and change in surface air temperature (ΔTAS). Correlations and trend lines are calculated using the 12-member ensemble only.

While we cannot rule out the possibility that interactions between OHU and SST in the tropics or SST and SIC in the NH extratropics are important, we believe that the spread in TCR across our experiments is attributable to interactions between OHU, SST, and sea ice in the SO for the following reasons:

1. The prescribed OHU is the only difference across the ensemble, so it must ultimately be the cause of any substantial (i.e., greater than the internal variability of the model) difference
2. The variation in response across the ensemble is concentrated in the SH extratropics (Fig. 3b), which strongly suggests that this region is the source of the variation
3. Considering the fact that CO_2 is doubled, the +ΔSIC runs have a very unrealistic SO cooling and increase in Antarctic sea ice (Fig. 3e), suggesting that a more moderate version of the same unrealistic SST cooling and sea ice growth processes could be occurring in all runs

Indeed, the three +ΔSIC runs produce a colder response than all CMIP5 models, and the CNRM-CM5 Q-flux run has an especially unrealistic temperature change of −0.8 K in response to doubled CO_2 and the prescribed OHU. This could be the result of an unrealistic combination of large OHU and shallow mixed-layer depth, particularly near areas inconsistent with the sea ice edge in CESM1-SOM, leading to sea ice growth. If this mechanism is present in the +ΔSIC runs, it is possible that the same mechanism is responsible for generating some of the spread in TCR across

Accepted for publication in *Journal of Climate*. DOI 10.1175/JCLI-D-24-0164.1.

the 12-member ensemble. Although the details of the coupling among OHU, SST, and SIC are not clear in our experiments, we argue that it is still valuable to analyze the coupled mechanisms responsible for the spread in the temperature response.

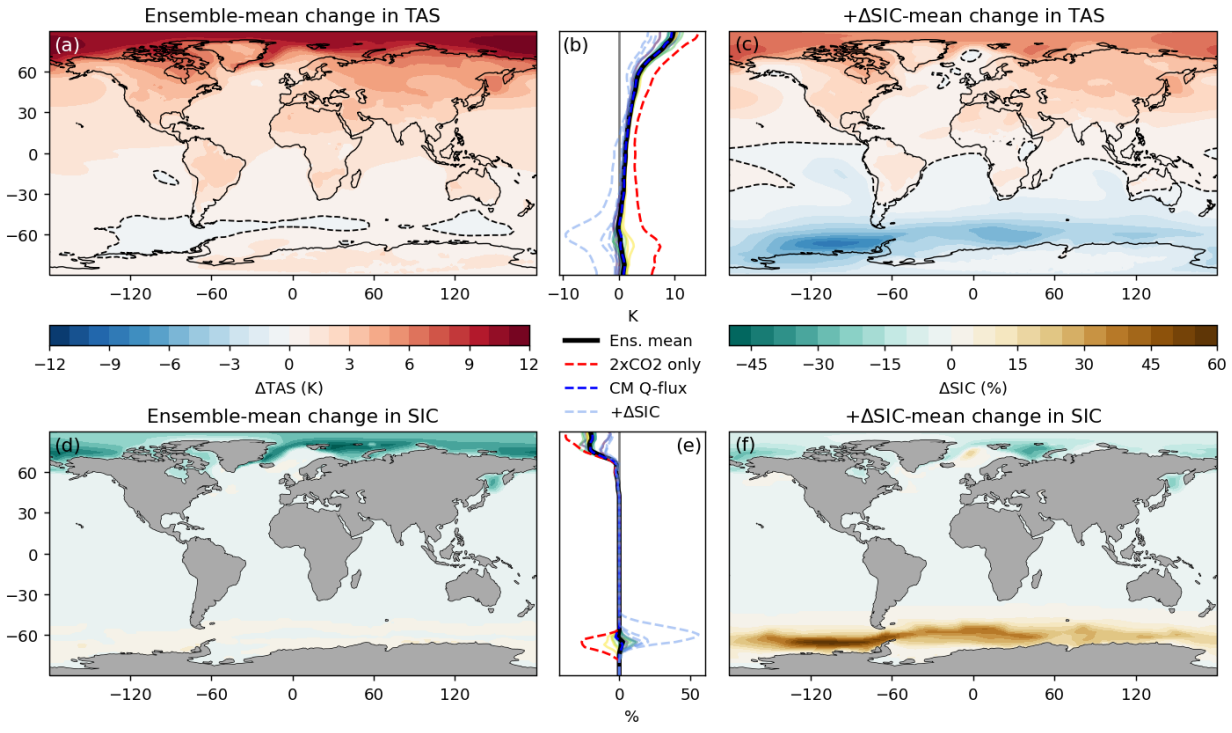

FIG. 3. 12-member ensemble-mean and +ΔSIC-mean changes in surface air temperature (TAS) and sea ice concentration (SIC) with zonal-mean plots for all experiments. The dashed black contour indicates the 0 K line for reference. Maps of the TAS and SIC responses for all experiments are shown in Figs. A2 and A3.

Figure 3 shows the 12-member ensemble-mean and 3-member +ΔSIC-mean changes in surface air temperature (TAS, used interchangeably with TCR for the 12-member ensemble) and sea ice concentration (SIC), along with the zonal-mean TAS and SIC response for each experiment. All runs can generally be characterized by enhanced Northern Hemisphere (NH) warming and reduced SH warming. By comparing the 2xCO2 only experiment (red dashed lines) to the TCR Q-flux forced experiments, we can see that most of the difference comes from either a reduction in Antarctic sea ice melting or sea ice expansion, accompanied by a reduced warming or a cooling of the SO. Some hemispheric asymmetry in the warming pattern is common in fully-coupled models under transient climate change because of the ability of the Southern Ocean to take up a relatively large

Accepted for publication in *Journal of Climate*. DOI 10.1175/JCLI-D-24-0164.1.

amount of heat and transport it equatorward (Armour et al. 2016). However, the large asymmetry present across these simulations results in a northward shift of the Hadley circulation, which is a well-documented response to the differential warming of the hemispheres across a variety of timescales (Schneider et al. 2014). The northward shift of the Hadley circulation is well-correlated with the hemispheric temperature difference across our experiments (Fig. 4). The substantial spread in response produced by the 12 ensemble members, plus the three cold outliers, allows us to explore the physical mechanisms linking changes in Antarctic sea ice to the global-mean temperature response through radiative feedbacks.

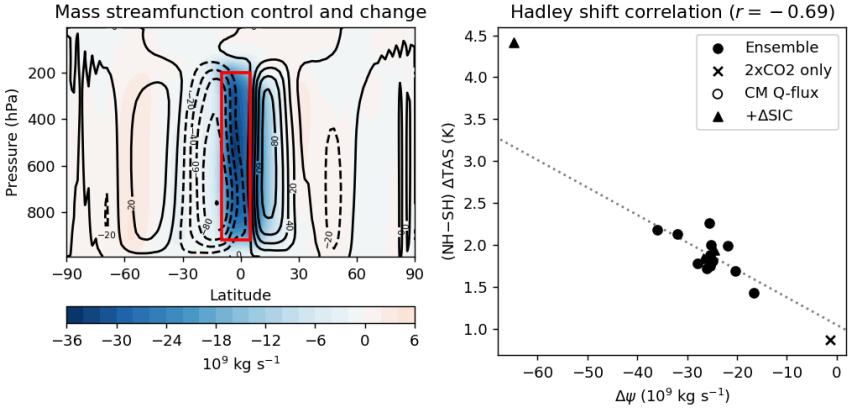

FIG. 4. Control (contours) and ensemble-mean change (shading) in mass streamfunction and correlation between northward Hadley circulation shift ($\Delta\psi$, calculated as the average mass streamfunction within the red box) and hemispheric temperature difference.

Accepted for publication in *Journal of Climate*. DOI 10.1175/JCLI-D-24-0164.1.

4. Feedback analysis

a. Radiative kernels

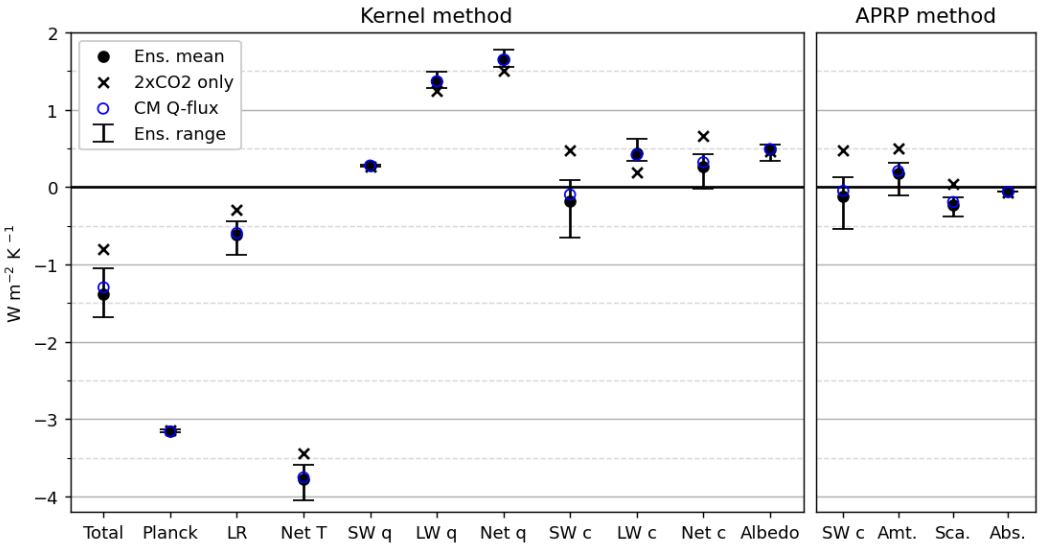

FIG. 5. Radiative feedbacks calculated using the radiative kernel method, including Planck, lapse rate (LR), and net temperature (Net T; sum of Planck and LR); SW, LW, and net water vapor (SW q, LW q, Net q); SW, LW, and net cloud (SW c, LW c, Net c); and surface albedo. Using the APRP method, the SW cloud feedback is calculated and decomposed into terms associated with cloud amount (Amt.), scattering (Sca.), and absorption (Abs.). Error bars indicate the 12-member ensemble range.

We first quantify the radiative feedbacks across the 12-member ensemble using the radiative kernel method (Soden et al. 2008) with the Pendergrass et al. (2018) kernels, which are generated from CESM1-CAM5. The largest spread in the feedbacks (indicated by the error bars in Fig. 5), as well as the largest difference between the ensemble and the 2xCO_2 only run, comes from the SW cloud feedback. The lapse rate feedback also contributes substantially to the TCR spread, but this is mainly an amplifying factor, as the Q-flux forced runs have heat removed from the slab ocean, leading to reduced warming at the surface and lower troposphere, especially in the SH midlatitudes. Because low cloud cover (thus the SW cloud feedback) is so strongly controlled by the stability of the lower troposphere (Bretherton 2015), this relatively large spread in the lapse rate feedback is tightly coupled to the SW cloud feedback. Therefore, we choose to focus our analysis on the cloud feedbacks.

Accepted for publication in *Journal of Climate*. DOI 10.1175/JCLI-D-24-0164.1.

Notably, the TCR spread is not generated by differences in surface albedo feedback, despite the wide range of sea ice response. The lack of spread in the albedo feedback parameter indicates that the effects surface albedo changes scale linearly with global mean temperature change, independent of the forcing mechanism. This is not the case for the SW cloud feedback. We interpret this difference in terms of local versus non-local feedback mechanisms. Contributions to the global albedo feedback originate primarily from grid cells that lose (or gain) sea ice. On the other hand, clouds far from the ice edge may respond non-locally to SST and SIC changes through atmospheric teleconnections that are sensitive to spatial patterns, in addition to purely local effects.

The top row of Fig. 6 shows the zonal-mean SW, LW, and net cloud feedbacks. While the SW and LW cloud feedbacks seem to be dominated by cloud changes in the tropics, they mostly cancel out, as shown in the net cloud feedback. This cancellation between LW and SW cloud feedbacks in the tropics accompanying a shift in the Hadley circulation has been noted in previous modeling studies, including asymmetrically-forced slab ocean models (Kang et al. 2008; Yoshimori and Broccoli 2009; Frierson and Hwang 2012; Voigt et al. 2017).

In the SH midlatitudes, the LW cloud feedback only weakly opposes the SW cloud feedback. What is left is a spread in the negative net cloud feedback in the SH midlatitudes, which is substantially different from the positive net cloud feedback in the 2xCO2 only run (red dashed line). In other words, the variation in the net cloud feedback is dominated by variation in the SW cloud feedback, largely localized to the SH midlatitudes. By comparison, all runs have a positive SW and net cloud feedback in the NH midlatitudes. Figure 6g shows the high correlation between the average SH midlatitude SW cloud feedback and TCR. This implies a strong coupling between the state of SH polar region and the low clouds of the midlatitudes, even on the equatorward side of the storm tracks.

Accepted for publication in *Journal of Climate*. DOI 10.1175/JCLI-D-24-0164.1.

b. Approximate partial radiative perturbation

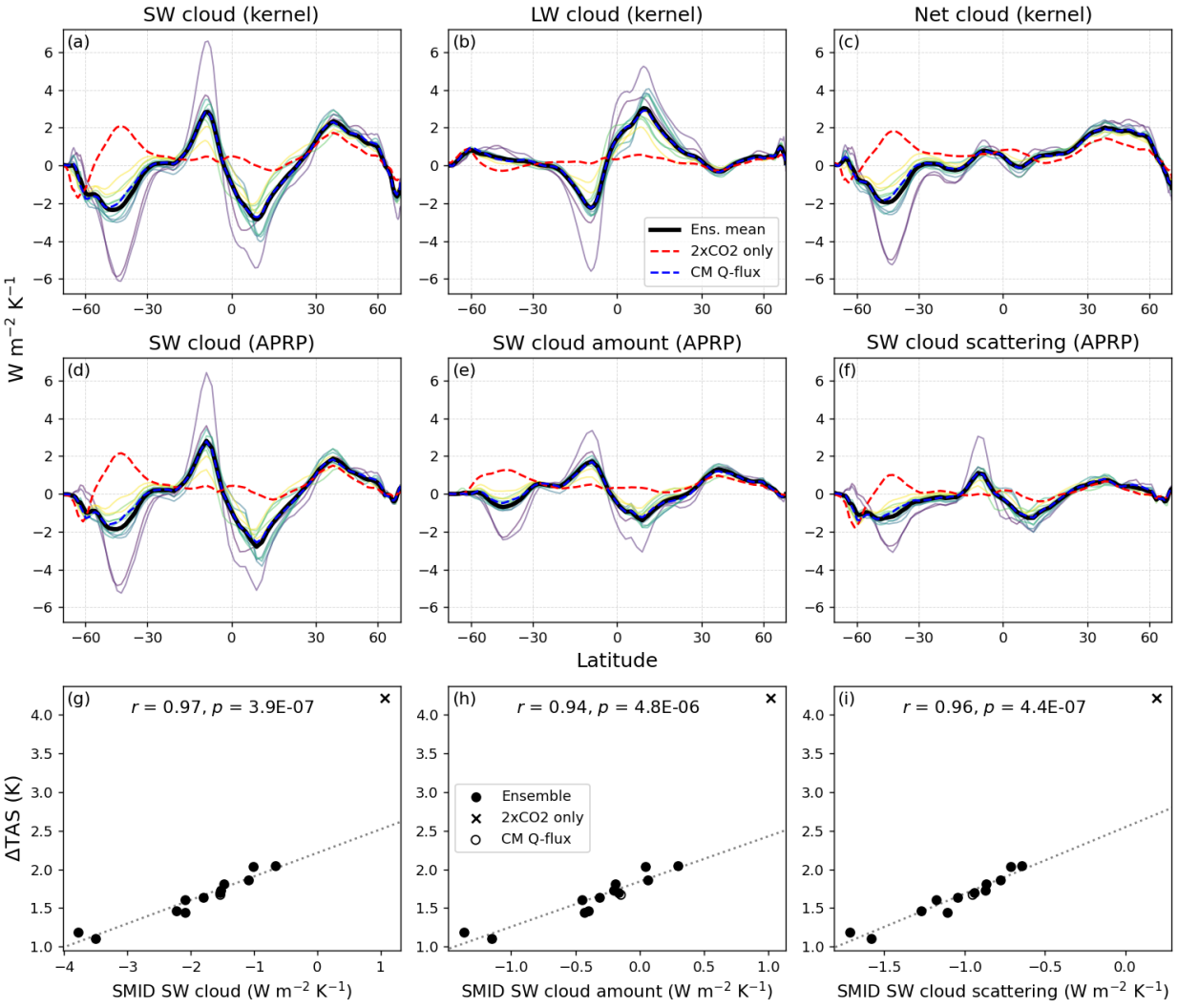

FIG. 6. (a–c) Zonal-mean SW, LW, and net cloud feedbacks by the radiative kernel method, (d–f) SW cloud feedback by the APRP method with decomposition into amount and scattering terms, and (g–i) correlations between the average SH midlatitude (SMID) SW cloud feedbacks (total, amount, and scattering) and the change in surface air temperature (ΔTAS).

We additionally apply the approximate partial radiative perturbation (APRP) method (Taylor et al. 2007; Zelinka 2023) to the 12-member ensemble for verification of the kernel method and in order to decompose the SW cloud feedback into terms representing changes in cloud fraction, scattering, and absorption. Figure 5 shows that the range of total SW cloud feedback is very similar

Accepted for publication in *Journal of Climate*. DOI 10.1175/JCLI-D-24-0164.1.

between the kernel and APRP methods. Comparing panels (a) and (d) of Fig. 6, the zonal mean SW cloud feedbacks obtained by the two methods are also very similar. In the SH midlatitudes, the SW cloud feedback can be explained in approximately equal measure by changes in cloud amount and scattering (brightness), while the absorption term (Fig. 5; zonal-mean not shown) is an order of magnitude smaller. The correlations between the SW cloud amount and scattering feedbacks and TCR are shown in Figs. 6h,i.

Both cloud amount and brightness have similar effects on the SW cloud feedback spread across the ensemble, with the coldest runs having the greatest increases in cloud amount and brightness across the SH midlatitudes, but their meridional structures are not identical (Figs. 6e,f). For the SW cloud amount feedback, we see a SH midlatitude-wide variation, but for the SW cloud scattering feedback, we see a dipole pattern centered around 50°S for some of the ensemble members. On the equatorward side of this dipole (i.e., 30–50°S), the amount and scattering components of the SW cloud feedback are very highly correlated ($r = 0.97$, not plotted).

5. Mechanisms behind spread in SW cloud feedback

Even though changes in both cloud amount and brightness are important contributions to the SW cloud feedback, our APRP results suggest that these cloud changes occur alongside each other across the ensemble, particularly within 30–50°S. That is, in regions where cloud cover increases/decreases, cloud brightness also increases/decreases, likely the result changes in cloud liquid water path as described by Kay et al. (2014) and Ceppi et al. (2016), who use the same model (CESM1-CAM5). Because of this apparent coupling between cloud amount and brightness, we choose to focus only on the changes associated with low cloud cover, which is closely linked to the SW cloud feedback (Klein et al. 2017).

Figure 7 shows the 12-member ensemble-mean change in low cloud cover, along with the zonal mean for all runs. There is an ensemble-mean increase in low cloud cover over the SH midlatitudes (outlined in black in Fig. 7a) and in the equatorial eastern Pacific and Atlantic. The SH midlatitude low cloud cover change is highly anticorrelated with TCR across the ensemble, as shown in Fig. 8a. There is also a general decrease in the NH midlatitude low cloud cover. The zonal-mean plots in Fig. 7b show the large spread in the SH midlatitude low cloud response across the ensemble

Accepted for publication in *Journal of Climate*. DOI 10.1175/JCLI-D-24-0164.1.

and in comparison to the hemispherically-symmetric decrease in the 2xCO2 only run, which is consistent with the feedback analysis of the previous section.

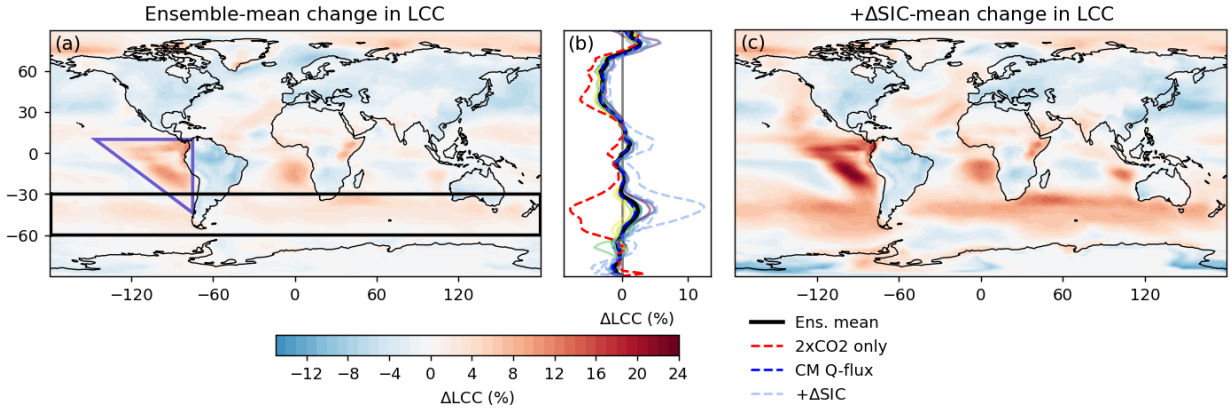

FIG. 7. 12-member ensemble-mean and +ΔSIC-mean change in low cloud cover (LCC) with zonal-mean plots of all experiments. Maps of the LCC response for all experiments are shown in Fig. A4.

The ensemble also displays large variations in low cloud cover over the eastern Pacific triangular region (EPT; outlined in blue in Fig. 7a). However, unlike the midlatitude changes, EPT cloud changes are not well-correlated with TCR (Fig. 8b). The low cloud cover in the region of the southeastern Atlantic that shows similarly large changes likewise has weak negative correlation with TCR ($r = -0.55$, not plotted). Previous studies within the pattern effect framework (e.g., Andrews et al. 2015; Ceppi and Gregory 2017; Andrews and Webb 2018; Dong et al. 2019, 2022) demonstrate the importance of changing low clouds in the EPT region for setting the pace of transient climate change, often expressed as the time-dependence of the global climate feedback parameter. While our results do not necessarily contradict these previous studies (considering our analysis is limited to one model), they do suggest that larger-scale changes in the SH midlatitude low clouds may be underappreciated in determining TCR, given their primary role across our experiments. There is some evidence of the teleconnection described by Kim et al. (2022) between the Southern Ocean and eastern Pacific based on the temperature and low cloud changes in the +ΔSIC runs (Figs. A2 and A4), where more extreme cold anomalies over the Southern Ocean are primarily advected over the eastern Pacific, leading to an increase in low clouds through stability.

Accepted for publication in *Journal of Climate*. DOI 10.1175/JCLI-D-24-0164.1.

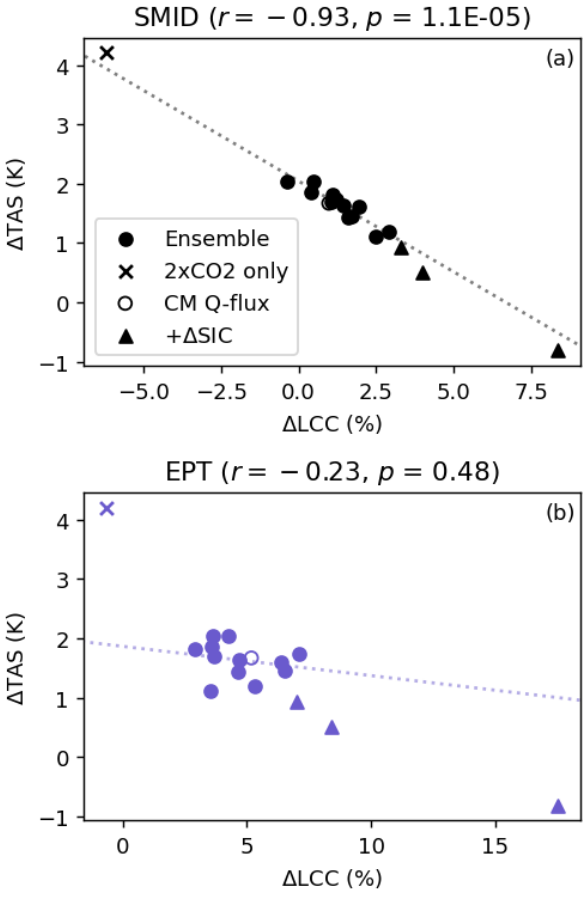

FIG. 8. Correlations between (a) SH midlatitude (SMID) and (b) EPT low cloud cover and global-mean ΔTAS. The SMID and EPT regions are outlined in Fig. 7a. Correlations, p-values, and trend lines are calculated using the 12-member ensemble only.

a. Cloud-controlling factors

To understand why the low clouds are changing, we first consider how changes in local environmental factors can influence cloud cover. Various cloud-controlling factors (CCFs) are used across the literature, but here we consider estimated inversion strength (EIS, as defined in Wood and Bretherton (2006)), 500-hPa vertical velocity (ω_{500}), near-surface wind speed (SWS), and SST, all calculated from monthly-mean data. Midlatitude low clouds have been shown to be sensitive to changes in EIS in observations (Wood and Bretherton 2006; Scott et al. 2020; Naud et al. 2023). Across the ensemble, the average SH midlatitude EIS is very well-correlated with low cloud cover over the same region (Fig. 9a), and a similarly strong relationship is present for

Accepted for publication in *Journal of Climate*. DOI 10.1175/JCLI-D-24-0164.1.

SST (Fig. 9d). Klein et al. (2017) discuss the possible issue of causality between changes in low clouds and changes in CCFs that are confined to the area around and below the low clouds (i.e., the boundary layer). An increase in low cloud can lead to cooler SSTs below and a further increase in stability, so despite the strong correlations between EIS/SSTs and low cloud cover, we cannot simply say that one causes the other without additional evidence, for example, from mechanism denial experiments.

Vertical velocity (Fig. 9b), as calculated from monthly-mean data, is not an important factor in determining midlatitude low cloud, in agreement with the observational results of Naud et al. (2023). This lack of correlation is likely for two reasons: (1) we use monthly-mean data, which averages over the vertical motion that would be important for the cloudiness of midlatitude storms, and (2) vertical velocity may not be an important factor in this midlatitude cloud regime (see for example Scott et al. 2020). The strong positive SWS correlation (Fig. 9c) may indicate the role of cold air advection into the region, but just as with vertical velocity, higher frequency data is likely required to make a conclusive statement (Scott et al. 2020). One drawback of our CCF analysis is that we do not control for the coupling of CCFs, such as the close correspondence of SST and EIS.

Accepted for publication in *Journal of Climate*. DOI 10.1175/JCLI-D-24-0164.1.

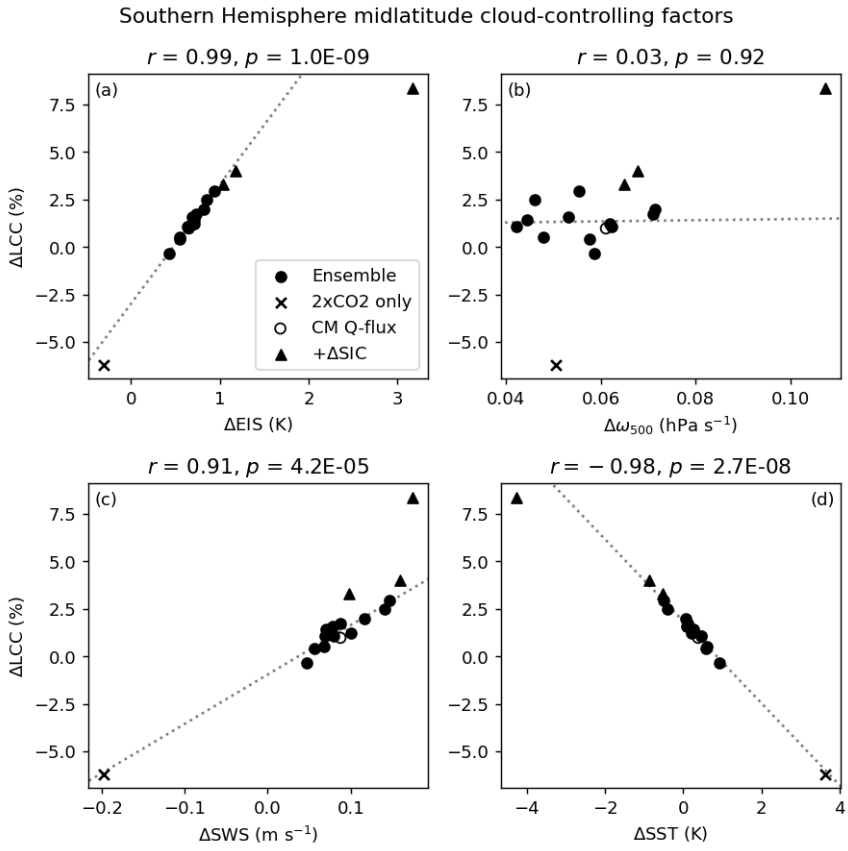

FIG. 9. Change in cloud-controlling factors: estimated inversion strength (EIS), 500-hPa vertical velocity (ω_{500}), near-surface wind speed (SWS), and sea surface temperature (SST) averaged over the SH midlatitudes plotted against change in SH midlatitude low cloud cover. The correlations, p-values, and trend lines are calculated using the 12-member ensemble only.

b. Baroclinicity and storm tracks

Since midlatitude low clouds are embedded within eddying storm tracks with significant sub-monthly variability, it is also of interest to look at metrics of storm track intensity. Here we will use column-integrated eddy kinetic energy (EKE) (Lehmann et al. 2014; Shaw et al. 2016; Chemke et al. 2022), calculated as follows:

$$\mathrm{EKE} = \int_{p_\mathrm{T}}^{p_0} (u'^2 + v'^2)\mathrm{d}p \tag{1}$$

Accepted for publication in *Journal of Climate*. DOI 10.1175/JCLI-D-24-0164.1.

where p_0 is a reference pressure (here 850 hPa), p_T is the pressure at the tropopause (here 250 hPa for simplicity), and u' and v' are the zonal and meridional winds associated with transient eddies.

Across nearly all experiments, EKE generally decreases in the NH midlatitudes (Fig. 10), corresponding to the decrease in low clouds over the region. In the SH midlatitudes, we see an opposite-signed EKE response between the 2xCO2 only run and the runs with OHU applied, and there is a spread in the response of the 12-member ensemble such that the colder runs have a greater increase in SH midlatitude EKE. The largest EKE changes in the SH occur on the poleward side of the midlatitudes and into the polar region, but there is still some variation on the equatorward side, where the largest low cloud changes occur across the ensemble. Across all experiments, EKE is well-correlated with low cloud cover in the midlatitudes of both hemispheres (Fig. 11), which also implies correlation with the global-mean temperature response via Fig. 8a.

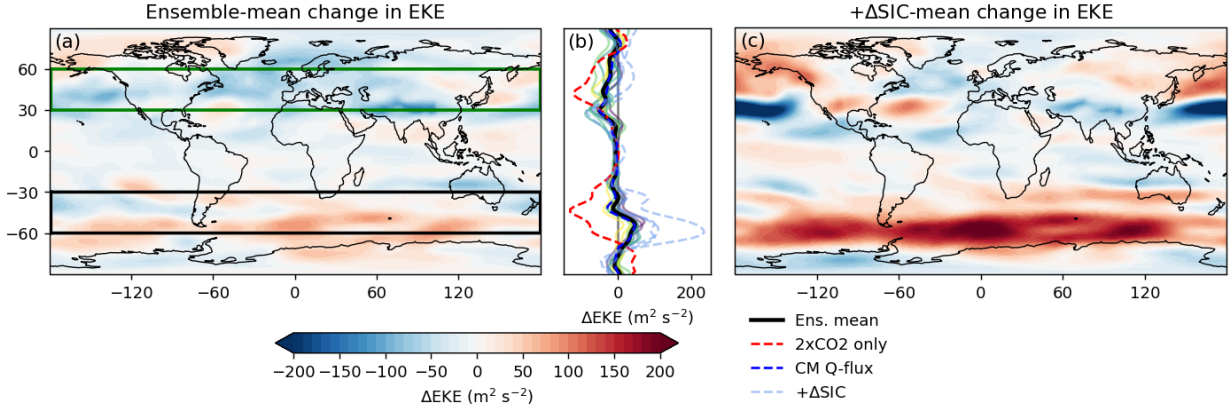

FIG. 10. 12-member ensemble-mean and +ΔSIC-mean change in EKE with zonal-mean plots for all experiments.

Accepted for publication in *Journal of Climate*. DOI 10.1175/JCLI-D-24-0164.1.

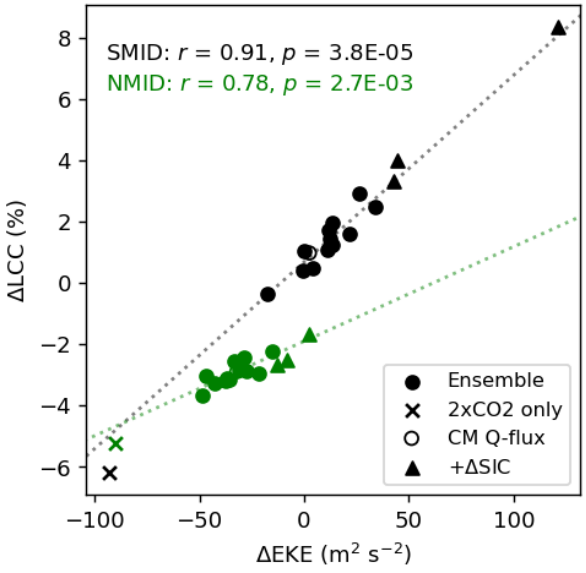

FIG. 11. Correlation between EKE and low cloud cover, both averaged over the NH (green) and SH (black) midlatitudes, indicated by the boxes in Fig. 10a. The correlations, p-values, and trend lines are calculated using the 12-member ensemble only.

Since changes in low clouds are known to occur alongside changes in lower-tropospheric stability and midlatitude circulation shifts (Grise and Medeiros 2016), it may be useful to consider the Eady growth rate, which is another common metric for baroclinicity and storm track intensity (Lehmann et al. 2014; Yuval and Kaspi 2020):

$$\sigma_{\mathrm{E}} = 0.31 \frac{\Lambda f}{N} \approx 0.31 \frac{g}{NT} \frac{\partial T}{\partial y} \tag{2}$$

where Λ is the vertical wind shear (where one may make an approximation through the thermal wind relation for the meridional temperature gradient $\partial T/\partial y$), f is the Coriolis parameter, and N is the Brunt–Väisälä frequency (Lindzen and Farrell 1980; Vallis 2017). The Eady growth rate (also integrated over 250–850 hPa) is well-correlated with EKE across the 12-member ensemble when averaged over the SH midlatitudes ($r = 0.82$, not shown), so it may provide a useful framework for understanding the storm track changes. As indicated by Eq. (2), there is an opposing influence of stability (N) and meridional temperature gradient ($\partial T/\partial y$) on baroclinicity. All else equal, we would expect a more stable midlatitude atmosphere to have weaker storm track intensity, but that

Accepted for publication in *Journal of Climate*. DOI 10.1175/JCLI-D-24-0164.1.

ignores the complex coupling between clouds, radiation, and circulation (Voigt et al. 2021). A detailed analysis of this coupling is beyond the scope of this work, but we can at least say that the impact of the change in the meridional temperature gradient on baroclinicity outweighs any influence from stability changes.

Similar to the relationship with stability, low clouds are strongly coupled to the midlatitude circulation. For example, Tselioudis and Rossow (2006) found that greater midlatitude storm strength is associated with a SW cooling effect. At the same time, absorbed SW radiation changes associated with cloud cover and brightness changes can increase the meridional temperature gradient, thus midlatitude baroclinicity (Ceppi et al. 2014). We propose that the low cloud cover response here can be explained by this positive low cloud–baroclinicity feedback, along with the previously discussed positive low cloud–stability feedback. While we focus on the SH because of its importance in the experiments studied in this paper, these arguments might also be applicable to the NH, at least over the ocean.

6. Summary and discussion

In this study, we prescribed an ensemble of OHU patterns to a slab ocean model under doubled CO_2, generating a range of climate states representing different hypothetical transient warming scenarios in a single model, with substantial differences in sea ice and global-mean temperature. In particular, the runs in which Antarctic sea ice was maintained or expanded had a significantly cooler SO compared to the 2xCO2 only run, which had a climatological (i.e., equilibrated) heat flux divergence boundary condition applied. In the slab ocean model, imposed Southern Ocean heat uptake near the sea ice edge or around areas with an unrealistically shallow mixed layer promoted cooling of SO SSTs and sea ice expansion. This led to a local cooling directly and through surface albedo changes, and the cold anomaly could likely be sustained by the continual prescribed heat uptake over the Southern Ocean. While the rest of the planet warmed in response to the CO_2 forcing, the SH extratropics were kept relatively cold, leading to an increase in the meridional temperature gradient of the SH.

Through a radiative feedback analysis, we found that the spread in the response was primarily determined by the SW cloud feedback in the SH midlatitudes, which is particularly evident when comparing the feedback strengths between our "transient" (i.e., CO_2 + OHU) and equilibrium

Accepted for publication in *Journal of Climate*. DOI 10.1175/JCLI-D-24-0164.1.

(CO_2 only) states. Changes in SH midlatitude low clouds are likely the result of changes in both stability and baroclinicity (via meridional temperature gradients) over the SH, but the causality is not clear, considering the coupling between clouds, radiation, and circulation. Because of the unrealistic cooling and sea ice growth in some of the runs, we assume that the SO SST and sea ice responses are primarily a cause, not an effect, of the circulation and cloud responses. This is a remote mechanism by which high-latitude SST and sea ice changes can drive a same-signed global-mean temperature change via the radiative effects of midlatitude low clouds.

While this ensemble is not meant to represent a best estimate of Earth's actual TCR, it does represent a plausible range of TCR, given the uncertainties in the future trends of SH temperature and sea ice. This ensemble demonstrates the importance of the Antarctic sea ice response in setting the course of transient climate change, as it can set up remote changes in midlatitude clouds which in turn have significant impact on global-mean temperature. Cloud-locking experiments (e.g., Grise et al. 2019) that break this coupling would allow us to make claims about causality. In particular, we plan to investigate regional locking of the SH midlatitude clouds in order to quantify how much cloud radiative effects feed back into stability and baroclinicity changes.

The use of a slab ocean model is a limitation because changes in ocean circulation would likely result in a different magnitude of response, as the ocean works to counter circulation shifts (England et al. 2020). The slab ocean model also clearly breaks the coupling between OHU and sea ice, but more work is required to understand how OHU excites a sea ice response and how it changes over a transient climate change scenario.

Limiting this study to one model only allowed us to focus on the role of OHU, SST, and sea ice changes in determining cloud feedbacks without the additional structural uncertainty in cloud process representation across models. This is a strength of our study, but investigating the robustness of our findings across models would be desirable. For a qualitative comparison, we can turn to one of the experiments from the Extratropical–Tropical Interaction Model Intercomparison Project (ETIN-MIP) in which an ensemble of fully-coupled models have reduced insolation prescribed over the SO (Kang et al. 2019). As expected from such an experiment, there is a global cooling, with the greatest cooling occurring over the SH extratropics (see their Fig. 4c). There is also a resulting increase in both Antarctic sea ice and SH midlatitude low cloud across the ensemble (see their Figs. 10c,f), which qualitatively agrees with our results. While the ETIN-MIP experiments

Accepted for publication in *Journal of Climate*. DOI 10.1175/JCLI-D-24-0164.1.

are nominally different from those described in this paper (changes in solar radiation as opposed to OHU), they are energetically very similar—energy is being removed from the SO surface. Although our experiments have global, spatially-complex forcings with significant North Atlantic components, the SH response of our experiments could be interpreted as the superposition of CO_2 forcing and the SH extratropical ETIN-MIP forcing.

In this work we have shown that the low cloud cover over the storm track region of the SH midlatitudes can exert a profound effect on global-mean temperature, and that these clouds are remotely shaped by teleconnections to high-latitude SO SSTs and Antarctic sea ice. It is possible that trends in the Antarctic play an underappreciated role in setting the planetary albedo through this remote cloud mechanism, both in models and in the real world. Given the substantial uncertainties in the drivers of SO SST and Antarctic sea ice changes over the historical period, we suggest prioritizing further study of the causal mechanisms linking SST, sea ice, atmospheric circulation, and midlatitude clouds.

Accepted for publication in *Journal of Climate*. DOI 10.1175/JCLI-D-24-0164.1.

Acknowledgments. We thank two anonymous reviewers for their thoughtful comments which helped clarify our work. This work was supported by NSF Awards AGS-1455071 and ICER-2026863. We would like to acknowledge high-performance computing support from Cheyenne (CISL 2019) provided by NCAR's Computational and Information Systems Laboratory, sponsored by the National Science Foundation.

Data availability statement. Model output will be made accessible through a University at Albany public data server, and Jupyter Notebooks that reproduce all figures will be available in a GitHub repository (https://github.com/r-ford/FRR-24).

APPENDIX

Forcing and response maps

For reference, we plot maps of the CMIP5 OHU anomalies which are added to the CESM1-CAM5 climatological Q-flux in Fig. A1. Maps of changes in surface air temperature, sea ice concentration, and low cloud cover for all experiments are plotted in Figs. A2, A3, and A4.

Accepted for publication in *Journal of Climate*. DOI 10.1175/JCLI-D-24-0164.1.

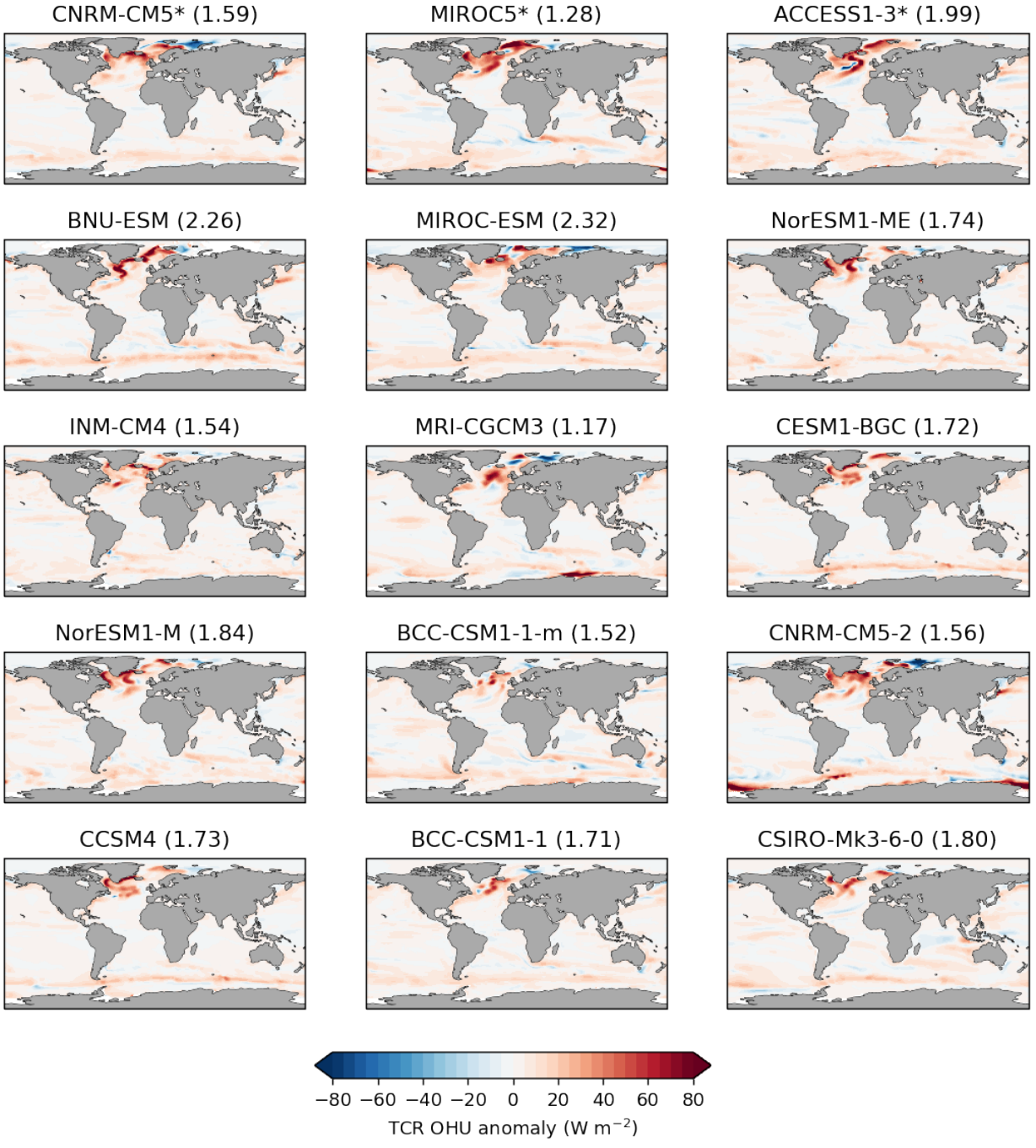

FIG. A1. Q-flux forcing patterns calculated from the CMIP5 models. Global-mean values (in W m^{-2}) are in parentheses next to the model names. Asterisks denote the three patterns resulting in the +ΔSIC runs.

Accepted for publication in *Journal of Climate*. DOI 10.1175/JCLI-D-24-0164.1.

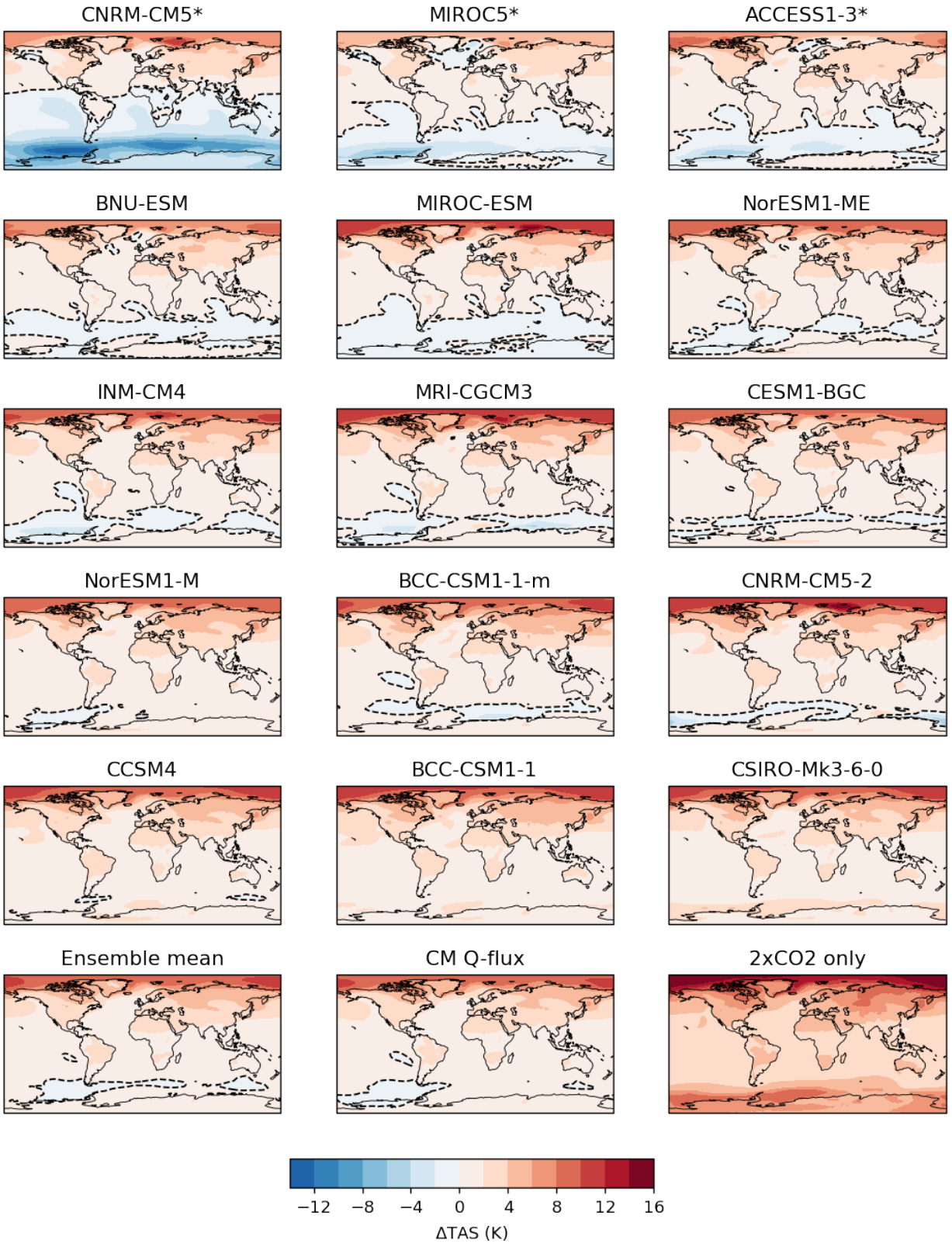

FIG. A2. Change in surface air temperature across the experiments. Asterisks denote the three +ΔSIC runs, and the dashed black contours indicate the 0 K line for reference. Zonal means are plotted in Fig. 3.

Accepted for publication in *Journal of Climate*. DOI 10.1175/JCLI-D-24-0164.1.

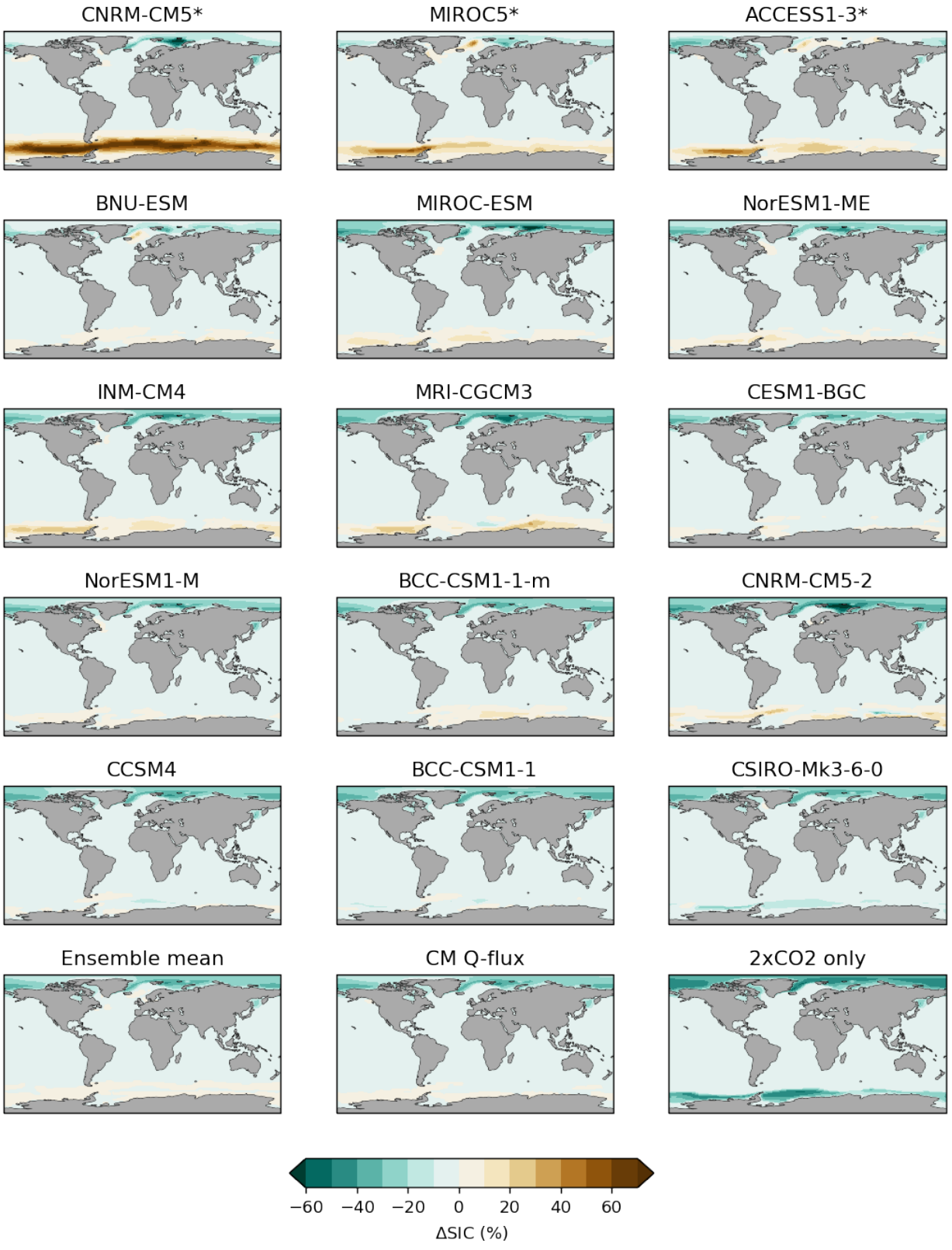

FIG. A3. As in Fig. A2, but for sea ice concentration.

Accepted for publication in *Journal of Climate*. DOI 10.1175/JCLI-D-24-0164.1.

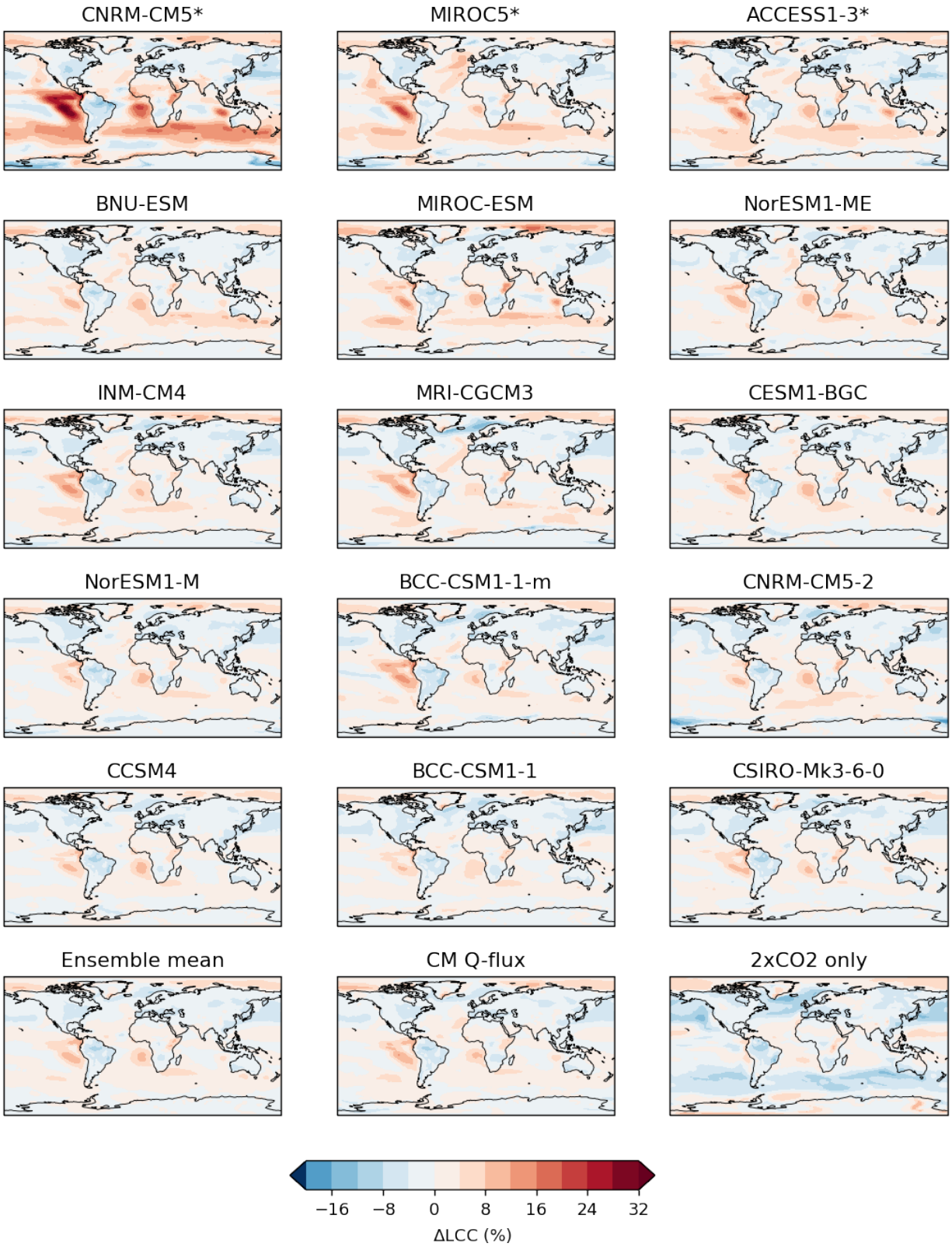

FIG. A4. As in Fig. A2, but for low cloud cover. Zonal means are plotted in Fig. 7.

Accepted for publication in *Journal of Climate*. DOI 10.1175/JCLI-D-24-0164.1.

References

Andrews, T., J. M. Gregory, and M. J. Webb, 2015: The Dependence of Radiative Forcing and Feedback on Evolving Patterns of Surface Temperature Change in Climate Models. *Journal of Climate*, **28 (4)**, 1630–1648, https://doi.org/10.1175/JCLI-D-14-00545.1.

Andrews, T., and M. J. Webb, 2018: The Dependence of Global Cloud and Lapse Rate Feedbacks on the Spatial Structure of Tropical Pacific Warming. *Journal of Climate*, **31 (2)**, 641–654, https://doi.org/10.1175/JCLI-D-17-0087.1.

Armour, K. C., J. Marshall, J. R. Scott, A. Donohoe, and E. R. Newsom, 2016: Southern Ocean warming delayed by circumpolar upwelling and equatorward transport. *Nature Geoscience*, **9 (7)**, 549–554, https://doi.org/10.1038/ngeo2731.

Bretherton, C. S., 2015: Insights into low-latitude cloud feedbacks from high-resolution models. *Philosophical Transactions of the Royal Society A: Mathematical, Physical and Engineering Sciences*, **373 (2054)**, 20140 415, https://doi.org/10.1098/rsta.2014.0415.

Ceppi, P., and J. M. Gregory, 2017: Relationship of tropospheric stability to climate sensitivity and Earth's observed radiation budget. *Proceedings of the National Academy of Sciences*, **114 (50)**, 13 126–13 131, https://doi.org/10.1073/pnas.1714308114.

Ceppi, P., and D. L. Hartmann, 2015: Connections Between Clouds, Radiation, and Midlatitude Dynamics: a Review. *Current Climate Change Reports*, **1 (2)**, 94–102, https://doi.org/10.1007/s40641-015-0010-x.

Ceppi, P., D. L. Hartmann, and M. J. Webb, 2016: Mechanisms of the Negative Shortwave Cloud Feedback in Middle to High Latitudes. *Journal of Climate*, **29 (1)**, 139–157, https://doi.org/10.1175/JCLI-D-15-0327.1.

Ceppi, P., M. D. Zelinka, and D. L. Hartmann, 2014: The response of the Southern Hemispheric eddy-driven jet to future changes in shortwave radiation in CMIP5. *Geophysical Research Letters*, **41 (9)**, 3244–3250, https://doi.org/10.1002/2014GL060043.

Chemke, R., Y. Ming, and J. Yuval, 2022: The intensification of winter mid-latitude storm tracks in the Southern Hemisphere. *Nature Climate Change*, **12 (6)**, 553–557, https://doi.org/10.1038/s41558-022-01368-8.

Accepted for publication in *Journal of Climate*. DOI 10.1175/JCLI-D-24-0164.1.

Chung, E.-S., and Coauthors, 2022: Antarctic sea-ice expansion and Southern Ocean cooling linked to tropical variability. *Nature Climate Change*, **12 (5)**, 461–468, https://doi.org/10.1038/s41558-022-01339-z.

CISL, 2019: *Cheyenne: HPE/SGI ICE XA System (University Community Computing)*. Boulder, CO, National Center for Atmospheric Research, https://doi.org/10.5065/D6RX99HX.

Danabasoglu, G., and P. R. Gent, 2009: Equilibrium Climate Sensitivity: Is It Accurate to Use a Slab Ocean Model? *Journal of Climate*, **22 (9)**, 2494–2499, https://doi.org/10.1175/2008JCLI2596.1.

Dong, Y., K. C. Armour, M. D. Zelinka, C. Proistosescu, D. S. Battisti, C. Zhou, and T. Andrews, 2020: Intermodel Spread in the Pattern Effect and Its Contribution to Climate Sensitivity in CMIP5 and CMIP6 Models. *Journal of Climate*, **33 (18)**, 7755–7775, https://doi.org/10.1175/JCLI-D-19-1011.1.

Dong, Y., A. G. Pauling, S. Sadai, and K. C. Armour, 2022: Antarctic Ice-Sheet Meltwater Reduces Transient Warming and Climate Sensitivity Through the Sea-Surface Temperature Pattern Effect. *Geophysical Research Letters*, **49 (24)**, e2022GL101 249, https://doi.org/10.1029/2022GL101249.

Dong, Y., C. Proistosescu, K. C. Armour, and D. S. Battisti, 2019: Attributing Historical and Future Evolution of Radiative Feedbacks to Regional Warming Patterns using a Green's Function Approach: The Preeminence of the Western Pacific. *Journal of Climate*, **32 (17)**, 5471–5491, https://doi.org/10.1175/JCLI-D-18-0843.1.

Dufresne, J.-L., and S. Bony, 2008: An Assessment of the Primary Sources of Spread of Global Warming Estimates from Coupled Atmosphere–Ocean Models. *Journal of Climate*, **21 (19)**, 5135–5144, https://doi.org/10.1175/2008JCLI2239.1.

England, M. R., L. M. Polvani, L. Sun, and C. Deser, 2020: Tropical climate responses to projected Arctic and Antarctic sea-ice loss. *Nature Geoscience*, **13 (4)**, 275–281, https://doi.org/10.1038/s41561-020-0546-9.

Flato, G., and Coauthors, 2013: Evaluation of Climate Models. *Climate Change 2013: The Physical Science Basis. Contribution of Working Group I to the Fifth Assessment Report of the*

Accepted for publication in *Journal of Climate*. DOI 10.1175/JCLI-D-24-0164.1.

Intergovernmental Panel on Climate Change, T. Stocker, D. Qin, G.-K. Plattner, M. Tignor, S. Allen, J. Boschung, A. Nauels, Y. Xia, V. Bex, and P. Midgley, Eds., Cambridge University Press, Cambridge, United Kingdom and New York, NY, USA, 741–866, https://doi.org/10.1017/CBO9781107415324.020, URL http://www.climatechange2013.org, section: 9 Type: Book Section.

Forster, P., and Coauthors, 2021: The Earth's Energy Budget, Climate Feedbacks, and Climate Sensitivity. *Climate Change 2021: The Physical Science Basis. Contribution of Working Group I to the Sixth Assessment Report of the Intergovernmental Panel on Climate Change*, V. Masson-Delmotte, P. Zhai, A. Pirani, S. Connors, C. Péan, S. Berger, N. Caud, Y. Chen, L. Goldfarb, M. Gomis, M. Huang, K. Leitzell, E. Lonnoy, J. Matthews, T. Maycock, T. Waterfield, O. Yelekçi, R. Yu, and B. Zhou, Eds., Cambridge University Press, Cambridge, United Kingdom and New York, NY, USA, 923–1054, https://doi.org/10.1017/9781009157896.009, type: Book Section.

Frierson, D. M. W., and Y.-T. Hwang, 2012: Extratropical Influence on ITCZ Shifts in Slab Ocean Simulations of Global Warming. *Journal of Climate*, **25 (2)**, 720–733, https://doi.org/10.1175/JCLI-D-11-00116.1.

Grise, K. M., and B. Medeiros, 2016: Understanding the Varied Influence of Midlatitude Jet Position on Clouds and Cloud Radiative Effects in Observations and Global Climate Models. *Journal of Climate*, **29 (24)**, 9005–9025, https://doi.org/10.1175/JCLI-D-16-0295.1.

Grise, K. M., B. Medeiros, J. J. Benedict, and J. G. Olson, 2019: Investigating the Influence of Cloud Radiative Effects on the Extratropical Storm Tracks. *Geophysical Research Letters*, **46 (13)**, 7700–7707, https://doi.org/10.1029/2019GL083542.

Hartmann, D. L., 2022: The Antarctic ozone hole and the pattern effect on climate sensitivity. *Proceedings of the National Academy of Sciences*, **119 (35)**, e2207889 119, https://doi.org/10.1073/pnas.2207889119.

Hwang, Y.-T., S.-P. Xie, C. Deser, and S. M. Kang, 2017: Connecting tropical climate change with Southern Ocean heat uptake. *Geophysical Research Letters*, **44 (18)**, 9449–9457, https://doi.org/10.1002/2017GL074972.

Accepted for publication in *Journal of Climate*. DOI 10.1175/JCLI-D-24-0164.1.

Kang, S. M., P. Ceppi, Y. Yu, and I.-S. Kang, 2023: Recent global climate feedback controlled by Southern Ocean cooling. *Nature Geoscience*, **16 (9)**, 775–780, https://doi.org/10.1038/s41561-023-01256-6.

Kang, S. M., I. M. Held, D. M. W. Frierson, and M. Zhao, 2008: The Response of the ITCZ to Extratropical Thermal Forcing: Idealized Slab-Ocean Experiments with a GCM. *Journal of Climate*, **21 (14)**, 3521–3532, https://doi.org/10.1175/2007JCLI2146.1.

Kang, S. M., and Coauthors, 2019: Extratropical–Tropical Interaction Model Intercomparison Project (Etin-Mip): Protocol and Initial Results. *Bulletin of the American Meteorological Society*, **100 (12)**, 2589–2606, https://doi.org/10.1175/BAMS-D-18-0301.1.

Kay, J. E., B. Medeiros, Y.-T. Hwang, A. Gettelman, J. Perket, and M. G. Flanner, 2014: Processes controlling Southern Ocean shortwave climate feedbacks in CESM. *Geophysical Research Letters*, **41 (2)**, 616–622, https://doi.org/10.1002/2013GL058315.

Kim, H., S. M. Kang, J. E. Kay, and S.-P. Xie, 2022: Subtropical clouds key to Southern Ocean teleconnections to the tropical Pacific. *Proceedings of the National Academy of Sciences*, **119 (34)**, e2200514 119, https://doi.org/10.1073/pnas.2200514119.

Klein, S. A., A. Hall, J. R. Norris, and R. Pincus, 2017: Low-Cloud Feedbacks from Cloud-Controlling Factors: A Review. *Surveys in Geophysics*, **38 (6)**, 1307–1329, https://doi.org/10.1007/s10712-017-9433-3.

Lee, S., M. L'Heureux, A. T. Wittenberg, R. Seager, P. A. O'Gorman, and N. C. Johnson, 2022: On the future zonal contrasts of equatorial Pacific climate: Perspectives from Observations, Simulations, and Theories. *npj Climate and Atmospheric Science*, **5 (1)**, 1–15, https://doi.org/10.1038/s41612-022-00301-2.

Lehmann, J., D. Coumou, K. Frieler, A. V. Eliseev, and A. Levermann, 2014: Future changes in extratropical storm tracks and baroclinicity under climate change. *Environmental Research Letters*, **9 (8)**, 084 002, https://doi.org/10.1088/1748-9326/9/8/084002.

Lindzen, R. S., and B. Farrell, 1980: A Simple Approximate Result for the Maximum Growth Rate of Baroclinic Instabilities. *Journal of the Atmospheric Sciences*, **37 (7)**, 1648–1654, https://doi.org/10.1175/1520-0469(1980)037⟨1648:ASARFT⟩2.0.CO;2.

Accepted for publication in *Journal of Climate*. DOI 10.1175/JCLI-D-24-0164.1.

Meehl, G. A., C. A. Senior, V. Eyring, G. Flato, J.-F. Lamarque, R. J. Stouffer, K. E. Taylor, and M. Schlund, 2020: Context for interpreting equilibrium climate sensitivity and transient climate response from the CMIP6 Earth system models. *Science Advances*, **6 (26)**, eaba1981, https://doi.org/10.1126/sciadv.aba1981.

Naud, C. M., G. S. Elsaesser, and J. F. Booth, 2023: Dominant Cloud Controlling Factors for Low-Level Cloud Fraction: Subtropical Versus Extratropical Oceans. *Geophysical Research Letters*, **50 (19)**, e2023GL104 496, https://doi.org/10.1029/2023GL104496.

Pendergrass, A. G., A. Conley, and F. M. Vitt, 2018: Surface and top-of-atmosphere radiative feedback kernels for CESM-CAM5. *Earth System Science Data*, **10 (1)**, 317–324, https://doi.org/10.5194/essd-10-317-2018.

Rose, B. E. J., K. C. Armour, D. S. Battisti, N. Feldl, and D. D. B. Koll, 2014: The dependence of transient climate sensitivity and radiative feedbacks on the spatial pattern of ocean heat uptake. *Geophysical Research Letters*, **41 (3)**, 1071–1078, https://doi.org/10.1002/2013GL058955.

Rose, B. E. J., and L. Rayborn, 2016: The Effects of Ocean Heat Uptake on Transient Climate Sensitivity. *Current Climate Change Reports*, **2 (4)**, 190–201, https://doi.org/10.1007/s40641-016-0048-4.

Rugenstein, M. A. A., K. Caldeira, and R. Knutti, 2016: Dependence of global radiative feedbacks on evolving patterns of surface heat fluxes. *Geophysical Research Letters*, **43 (18)**, 9877–9885, https://doi.org/10.1002/2016GL070907.

Rye, C. D., J. Marshall, M. Kelley, G. Russell, L. S. Nazarenko, Y. Kostov, G. A. Schmidt, and J. Hansen, 2020: Antarctic Glacial Melt as a Driver of Recent Southern Ocean Climate Trends. *Geophysical Research Letters*, **47 (11)**, e2019GL086 892, https://doi.org/10.1029/2019GL086892.

Sallée, J.-B., E. Shuckburgh, N. Bruneau, A. J. S. Meijers, T. J. Bracegirdle, and Z. Wang, 2013: Assessment of Southern Ocean mixed-layer depths in CMIP5 models: Historical bias and forcing response. *Journal of Geophysical Research: Oceans*, **118 (4)**, 1845–1862, https://doi.org/10.1002/jgrc.20157.

Accepted for publication in *Journal of Climate*. DOI 10.1175/JCLI-D-24-0164.1.

Schneider, T., T. Bischoff, and G. H. Haug, 2014: Migrations and dynamics of the intertropical convergence zone. *Nature*, **513 (7516)**, 45–53, https://doi.org/10.1038/nature13636.

Scott, R. C., T. A. Myers, J. R. Norris, M. D. Zelinka, S. A. Klein, M. Sun, and D. R. Doelling, 2020: Observed Sensitivity of Low-Cloud Radiative Effects to Meteorological Perturbations over the Global Oceans. *Journal of Climate*, **33 (18)**, 7717–7734, https://doi.org/10.1175/JCLI-D-19-1028.1.

Shaw, T. A., and Coauthors, 2016: Storm track processes and the opposing influences of climate change. *Nature Geoscience*, **9 (9)**, 656–664, https://doi.org/10.1038/ngeo2783.

Sherwood, S. C., and Coauthors, 2020: An Assessment of Earth's Climate Sensitivity Using Multiple Lines of Evidence. *Reviews of Geophysics*, **58 (4)**, e2019RG000 678, https://doi.org/10.1029/2019RG000678.

Soden, B. J., I. M. Held, R. Colman, K. M. Shell, J. T. Kiehl, and C. A. Shields, 2008: Quantifying Climate Feedbacks Using Radiative Kernels. *Journal of Climate*, **21 (14)**, 3504–3520, https://doi.org/10.1175/2007JCLI2110.1.

Taylor, K. E., M. Crucifix, P. Braconnot, C. D. Hewitt, C. Doutriaux, A. J. Broccoli, J. F. B. Mitchell, and M. J. Webb, 2007: Estimating Shortwave Radiative Forcing and Response in Climate Models. *Journal of Climate*, **20 (11)**, 2530–2543, https://doi.org/10.1175/JCLI4143.1.

Tselioudis, G., and W. B. Rossow, 2006: Climate feedback implied by observed radiation and precipitation changes with midlatitude storm strength and frequency. *Geophysical Research Letters*, **33 (2)**, https://doi.org/10.1029/2005GL024513.

Vallis, G. K., 2017: *Atmospheric and Oceanic Fluid Dynamics: Fundamentals and Large-Scale Circulation*. 2nd ed., Cambridge University Press.

Voigt, A., N. Albern, P. Ceppi, K. Grise, Y. Li, and B. Medeiros, 2021: Clouds, radiation, and atmospheric circulation in the present-day climate and under climate change. *WIREs Climate Change*, **12 (2)**, e694, https://doi.org/10.1002/wcc.694.

Voigt, A., and Coauthors, 2017: Fast and slow shifts of the zonal-mean intertropical convergence zone in response to an idealized anthropogenic aerosol. *Journal of Advances in Modeling Earth Systems*, **9 (2)**, 870–892, https://doi.org/10.1002/2016MS000902.

Accepted for publication in *Journal of Climate*. DOI 10.1175/JCLI-D-24-0164.1.

Wills, R. C. J., Y. Dong, C. Proistosecu, K. C. Armour, and D. S. Battisti, 2022: Systematic Climate Model Biases in the Large-Scale Patterns of Recent Sea-Surface Temperature and Sea-Level Pressure Change. *Geophysical Research Letters*, **49 (17)**, e2022GL100 011, https://doi.org/10.1029/2022GL100011.

Winton, M., K. Takahashi, and I. M. Held, 2010: Importance of Ocean Heat Uptake Efficacy to Transient Climate Change. *Journal of Climate*, **23 (9)**, 2333–2344, https://doi.org/10.1175/2009JCLI3139.1.

Wood, R., and C. S. Bretherton, 2006: On the Relationship between Stratiform Low Cloud Cover and Lower-Tropospheric Stability. *Journal of Climate*, **19 (24)**, 6425–6432, https://doi.org/10.1175/JCLI3988.1.

Yoshimori, M., and A. J. Broccoli, 2009: On the link between Hadley circulation changes and radiative feedback processes. *Geophysical Research Letters*, **36 (20)**, https://doi.org/10.1029/2009GL040488.

Yuval, J., and Y. Kaspi, 2020: Eddy Activity Response to Global Warming–Like Temperature Changes. *Journal of Climate*, **33 (4)**, 1381–1404, https://doi.org/10.1175/JCLI-D-19-0190.1.

Zelinka, M., 2023: mzelinka/aprp: April 7, 2023 Release. URL https://zenodo.org/records/7809085, https://doi.org/10.5281/zenodo.7809085.

Accepted for publication in *Journal of Climate*. DOI 10.1175/JCLI-D-24-0164.1.